Journal of Power Sources 196 (2011) 8931–8941

Contents lists available at ScienceDirect

Journal of Power Sources

journal homepage: www.elsevier.com/locate/jpowsour

Ni/YSZ anode – Effect of pre-treatments on cell degradation and microstructures

Anne Hauch*, Peter Stanley Jørgensen, Karen Brodersen, Mogens Mogensen

Fuel Cells and Solid State Chemistry Division, Risø National Laboratory for Sustainable Energy, Technical University of Denmark, Frederiksborgvej 399, DK-4000 Roskilde, Denmark

ARTICLE INFO

Article history:
Received 5 November 2010
Received in revised form
21 December 2010
Accepted 4 January 2011
Available online 13 January 2011

Keywords:
Ni/YSZ
Degradation
Impurities
Gas cleaning
Multilayer tape casting
Microstructure

ABSTRACT

Anode supported (Ni/YSZ–YSZ–LSM/YSZ) solid oxide fuel cells were tested and the degradation over hundreds of hours was monitored and analyzed by impedance spectroscopy. Test conditions were chosen to focus on the Ni/YSZ anode degradation and all tests were operated at 750 °C, a current density of 0.75 A cm^{-2}. Oxygen was supplied to the cathode and the anode inlet gas mixture had a high p(H_2O)/p(H_2) ratio of 0.4/0.6. Commercially available gasses were applied. The effect of different types of pre-treatments on the Ni/YSZ electrode degradation during subsequent fuel cell testing was investigated. Pre-treatments included operating at OCV (4% and 40% H_2O in H_2) prior to fuel cell testing, cleaning of the inlet H_2 gas at 700 °C and processing the anode half cell via multilayer tape casting. Analyses of impedance spectra showed that the increase in the charge transfer reaction resistance in the Ni/YSZ ($R_{Ni,TPB}$) was decreased to ¼ or less for the pre-treated and fuel cell tested cells when compared with a non-pre-treated reference tested cell; all operated at the same fuel cell test conditions. Scanning electron microscopy and image analyses for the non-pre-treated reference tested cell and selected pre-treated cells showed significant differences in the area fractions of percolating nickel both in the active anode and support layer.

1. Introduction

Over the last few decades solid oxide fuel cells (SOFC) have moved significantly closer to becoming a commercially mature energy conversion technology for which reliability, low production cost and long-term stability are important factors [1–3]. One of the most widely used materials for SOFC anodes is a porous cermet of nickel and yttria stabilized zirconia (YSZ). The Ni/YSZ cermet has some obvious advantages such as: (1) it is fully reversible, i.e. it works equally well in fuel cell and electrolysis mode [4], (2) it has excellent catalytic and electrocatalytic activity both for steam reforming of natural gas and for electrochemical oxidation of H_2 and CO, (3) the raw materials are abundant and therefore available at technological relevant prices [5,6]. However, there are also some well-known challenges for the long-term stability of the Ni/YSZ cermet as an SOFC anode e.g. its sensitivity towards poisoning; it is prone to carbon deposition and can show mechanical instability upon redox cycling [7–11]. In the perspective of technological relevance and future commercialization of SOFC, it is important to study the Ni/YSZ electrode degradation for technologically relevant cells and aim for decreasing or ideally preventing this Ni/YSZ degradation.

In literature the Ni/YSZ electrodes in full cells are reported to undergo an "initial" degradation within the first few hours of testing (the exact time frame depends on the cells and the exact test conditions) and reach a certain performance plateau. This observed increase in the resistance of the Ni/YSZ electrodes follow an exponential trend that can be described by an equation of the form: $R_{Ni,TPB}(t) = R_{Ni,0} + \Delta R \cdot [1 - \exp(-t/\tau)]$, where $R_{Ni,0}$ and ΔR, are the initial value and total increase for the Ni–YSZ charge transfer reaction resistance and τ is the characteristic time for the Ni/YSZ electrode degradation [12–16]. Some authors have argued that there is a close relationship between the observed Ni/YSZ degradation and Ni particle growth, or more specifically the decrease in triple-phase-boundaries (TPB) that is the consequence of the Ni particle growth [15–17].

Previously we have reported results on the effect of p(H_2O)/p(H_2) on the expression for the increase in the Ni/YSZ charge transfer reaction resistance, $R_{Ni,TPB}(t) = R_{Ni,0} + \Delta R \cdot [1 - \exp(-t/\tau)]$, and shown that the main factor changing upon changing the p(H_2O)/p(H_2) is the characteristic time, τ, for the Ni/YSZ electrode degradation [13]. Inspired by interesting results when applying gas cleaning for electrolysis testing of similar cells [18], we have also reported results on significant decrease in the Ni/YSZ electrode degradation obtained by cleaning of the inlet H_2 gas during fuel cell testing [19]. The present work is a continuation of previously reported fuel cell test results and similar anode supported full SOFCs have been tested in this work.

Here we report results from several fuel cell tests all conducted at a temperature of 750 °C and a current density of 0.75 A cm^{-2} applying O_2 to the cathode and 40% H_2O in H_2 to the anode (26% H_2

* Corresponding author. Tel.: +45 21362836; fax: +45 46775858.
E-mail address: hauc@risoe.dtu.dk (A. Hauch).

0378-7753/$ – see front matter © 2011 Elsevier B.V. All rights reserved.
doi:10.1016/j.jpowsour.2011.01.009

utilization). Except for one of the reported fuel cell tests, all tests were performed on similar anode supported Ni/YSZ–YSZ–LSM/YSZ cells. The aim of this work has been to investigate how the Ni/YSZ electrode degradation at the specified fuel cell test conditions is affected by: (1) different types of pre-treatments at OCV prior to fuel cell testing, (2) cleaning of the H_2 inlet gas at high temperature and (3) pre-treatment of the anode by processing the anode half cell via multilayer tape casting. Equivalent circuit modeling of impedance spectra (IS) and low voltage in-lens SEM imaging of selected cell pieces is applied in the analyses of the Ni/YSZ electrode degradation.

2. Experimental

2.1. Cell specifications

Anode supported Ni/YSZ–YSZ–LSM/YSZ cells produced at Risø DTU have been applied for tests A–E and these cells have been described previously [12,13,19–23]. For these anode supported cells the half cell was produced by tape casting of the anode support; hereafter a suspension of the active anode and a suspension of the electrolyte material was sprayed on the tape and the half cell was co-sintered [23]. These cells have a 10–15 μm thick anode of Ni/YSZ cermet with a ~300 μm thick Ni/YSZ support layer, a 10–15 μm thick YSZ electrolyte and a ~20 μm thick LSM–YSZ composite cathode [20]. The ratio between Ni and YSZ is 40/60 volume percentage both for the support layer and the active electrode layer [24]. ZrO_2 stabilized with 8 mole percentage Y_2O_3 is used for the electrolyte and the active electrode layer. ZrO_2 stabilized with 3 mole percentage Y_2O_3 is used for the support layer. The composition of the LSM is $(La_{0.75}Sr_{0.25})_{0.95}MnO_3$ and the ratio between LSM and YSZ in the composite electrode is LSM/YSZ = 50/50 volume percentage [25]. For production of the anode half cell for the cell used for test F, the procedure; (1) tape casting of anode support, (2) spraying of active anode and (3) spraying of electrolyte; was substituted by a multilayer tape casting process [26]. For this multilayer tape cast cell for test F, the electrolyte, the active anode layer and the anode support layer are all tape cast successive (i.e. all three layers wet-on-wet) followed by co-sintering of the half cell. The same raw materials, compositions, layer thickness, etc. were applied for the cell for test F as for the cells for tests A–E. The produced SOFC are all planar 12 cm × 12 cm cells which are cut into 5 cm × 5 cm cells prior to testing. Due to the set-up for cell testing, the cells have an active electrode area of 16 cm^2. The set-up for cell testing, i.e. alumina housing, current collectors (Ni and Au foil), glass sealing and Ni/YSZ and LSM based gas distributors, is illustrated and described in detail elsewhere [27,28]. Commercially available gasses from Air Liquide were used for all tests (oxygen: industrial grade, $O_2 \geq 99.5\%$ and hydrogen: N30, $H_2 \geq 99.9\%$). Impurities (e.g. hydrogen sulfide and water) has been detected by mass spectroscopy in these commercially available gasses generally used for cell testing in our laboratory; however the concentrations of impurities were too small to be properly quantified using mass spectrometry [18,29].

2.2. Test procedure and operating conditions

The general cell test sequence was: (1) heated to 1000 °C (1 °C/min) and sealed, (2) reduction of the NiO in the anode and support layer in 9% H_2 in N_2 and subsequently pure H_2 with 3% humidification, (3) the temperature lowered to 850 °C and characterization (leak testing, iV-curves and impedance spectroscopy) at different gas compositions and temperatures was performed. iV-curves and impedance spectra (IS) were recorded at 750 °C, 800 °C and 850 °C both with pure oxygen and with air to the cathode, and applying 4%, 20%, 40% and 50% H_2O in H_2 to the anode, i.e. at 24 different operating conditions. After characterization galvanostatic fuel cell testing was started at a temperature of 750 °C and a current density of 0.75 A cm^{-2}. The flow to the cathode was O_2 applying flow of 50 l h^{-1}) and the flow to the anode was 40% H_2O in H_2 (26% H_2 utilization). For all tests IS were recorded regularly (approximately twice per day) during testing to monitor the development of the cell impedance during the galvanostatic fuel cell tests. However, for simplicity we generally only show the first and last IS recorded during each fuel cell testing including results from the break-down of losses by applying the equivalent circuit model described in the next paragraph.

2.3. Impedance spectroscopy

IS were recorded using a Solartron 1260 frequency analyzer. For impedance measurements under current load, the Solartron 1260 was used in combination with an external shunt to measure the AC current through the cell [30]. The software Zview 2.8 was used for analyses of the IS [31]. To break down the losses of the impedance of the cells, the equivalent circuit model described by Barfod et al. for similar cells was applied [22]. This equivalent circuit model consists of an inductance (L) in series with a series resistance (R_s) and in series with the polarization resistance (R_p). R_p is built up by five circuits of a resistance (R) in parallel with a constant phase element (CPE). The five circuits represent a high frequency arc originating from the LSM/YSZ cathode, $(R,CPE)_{LSM,high}$; an arc originating from the charge transfer reactions resistance in the Ni/YSZ electrode, $(R,CPE)_{Ni,TPB}$; a low frequency arc originating from the LSM/YSZ cathode, $(R,CPE)_{LSM,low}$; a gas diffusion related arc, $(R,CPE)_{Diff}$; and a low frequency arc originating from gas conversion mainly due to the anode $(R,CPE)_{Conv.}$. The three arcs $(R,CPE)_{LSM,high}$; $(R,CPE)_{Ni,TPB}$; and $(R,CPE)_{LSM,low}$ describe the electrochemical processes in the cathode and anode. The relative errors $(Z_{fit} - Z_{exp})/Z_{exp}$ was calculated as a function of frequency for Z' and Z'' and were below 10% for the fitted spectra for frequencies down to below the summit frequency for the gas conversion arc i.e. below 3 Hz.

Gas change impedance spectroscopy was performed at OCV to obtain electrode-specific and model-independent impedance characterization of the cells as described in detail by Jensen et al. [32]. In this study the gas change for the cathode was between air and O_2, and for the anode between 4% and 20% H_2O in H_2. From the differences in the impedance upon gas changes values for $\delta\Delta Z'(f)$ were calculated as:

$$\delta\Delta Z'(f_n) = \frac{\left[Z'_{air}(f_{n+1}) - Z'_{air}(f_{n-1})\right] - \left[Z'_{O2}(f_{n+1}) - Z'_{O2}(f_{n-1})\right]}{\ln(f_{n+1}) - \ln(f_{n-1})} \quad (1)$$

for cathode gas change, where $Z'(f_{n+1})$ is the real part of the impedance measured at the $(n+1)$th frequency applying either air or O_2 to the cathode. In a similar way $\delta\Delta Z'(f)$ was calculated for the differences upon anode gas change.

2.4. Scanning electron microscopy (SEM) and image analysis

Pieces of a reference cell (which was reduced but not tested as a fuel cell) and pieces of cells from selected tests were subjected to field emission scanning electron microscopy (FE-SEM) imaging and subsequent image analyses. The cells were prepared for SEM investigation by vacuum embedding pieces of the cells in epoxy (EpoFix from Struers®) followed by grinding and polishing. A Zeiss Supra 35 FE-SEM and a Zeiss CrossBeam XB1540 were used for low-voltage SEM imaging using the in-lens detector in order to distinguish percolating and non-percolating Ni in the Ni/YSZ structure as described by Thydén et al. [33]. The image analyses, e.g. determination of the area fraction of percolating Ni, were obtained as follows on images at the same magnification level. Several images were selected from

Table 1
Test specifications. All tests were operated a temperature of 750 °C and a current density of 0.75 A cm^{-2}. The flow to the cathode was 50 l h^{-1} of O_2 and the flow to the anode was 40% H_2O in H_2 (26% H_2 utilization). For comparison of cell voltage degradation, the cell voltage degradation after 250 h of fuel cell testing is given for all tests.

Test no.	Duration [h]	$\Delta U_{250\,h}$ [mV]	Test specifications
A	256	70	Reference cell test [13]
B	264	18	Pre-treatment, 40% H_2O in H_2 at OCV for 440 h prior to fuel cell testing [19]
C	314	18	Pre-treatment, 4% H_2O in H_2 at OCV for 440 h prior to fuel cell testing [19]
D	286	13	Cleaning of H_2 inlet gas at 700 °C
E	310	13	Without cleaning of H_2 inlet gas after 286 h of fuel cell testing applying cleaning of H_2 inlet gas at 700 °C (test D)
F	244	14	Reference cell test for a cell having a multilayer tape cast anode half cell

each cell where each image contained both the electrolyte – anode interface and the anode – support layer interface (similar to the images a, b, d and e in Fig. 9). Two horizontal lines were defined by hand, the first at the electrolyte/anode interface (line L_{ea}) as far into the anode as to not include any parts of the electrolyte. The second line was defined at the anode/support layer interface (line L_{as}). A histogram of intensities in the image from the L_{ea} line and up was then plotted. All the histograms showed two peaks, one for the percolating Ni and one for all other phases. A simple threshold was defined manually at the location between these two peaks with the lowest frequency. The threshold was then applied to the image to segment the percolating Ni from the background. The pixels between the L_{ea} and the L_{as} where denoted as belonging to the active anode and the pixels above the L_{as} line were denoted as belonging to the anode support. The percolating Ni fraction was then calculated for each of these two pixel regions as the number of Ni pixels in the segmentation divided by the total number of pixels in the region.

3. Results

After reduction and initial characterization of the full cells, long-term galvanostatic fuel cell testing was started. Table 1 gives an overview of the fuel cell tests, the test durations, cell voltage degradation after 250 h and the test specifications. Test A can be considered a reference cell test. Results and analysis of IS for tests A and B is given elsewhere [13,19], but the cell voltage curve is included here for comparison. Tests B and C were both subjected to 440 h of operation at OCV at 750 °C and at 40% and 4% H_2O in H_2, respectively, prior to fuel cell testing. As reported previously [19] the polarization resistance reached a constant value after 440 h of OCV testing at 40% H_2O in H_2 for test B, and therefore the OCV pre-treatment was stopped. To emphasize the steam content during OCV pre-treatment, the OCV pre-treatment for test C was also stopped after 440 h, and fuel cell testing was started. For test D the inlet H_2 gas was supplied through porous Ni at 700 °C in an attempt to clean the hydrogen prior to the inlet tubing for the anode compartment of the cell [34]. After operating test D at constant conditions for 286 h the gas cleaning system was by-passed, the cell was characterized at different temperatures and gas compositions and then fuel cell test E was started without gas cleaning on the same cell as for test D. Fig. 1 shows the cell voltage curve over time during fuel cell testing at 750 °C and a current density of 0.75 A cm^{-2}. The cells used for tests A–E are identical from a production point of view and part of the variations in the measured ohmic resistance (R_s) from IS (Table 3) at start up of fuel cell testing can originate from the set-up (auxiliary components, contacting, etc.) [35]. The differences in R_s values for tests C–E compared to reference test A was 0.018 Ω cm^2, 0.020 Ω cm^2, 0.014 Ω cm^2, respectively. These differences in R_s values correspond to 13 mV (test C), 15 mV (test D) and 11 mV (test E) at 0.75 A cm^{-2}. In Fig. 1 a value of 13 mV, 15 mV and 11 mV was added to the cell voltage curve for tests C–E, respectively, which made the comparison of the cell voltage curves in Fig. 1 more direct. The cell used for test F was significantly different from a production/processing point of view and therefore a correction of the cell voltage in accordance with the measured R_s value was not done for the test F in Fig. 1. It is evident from the cell voltage curves in Fig. 1 and Table 1 that the voltage degradation for test A is significantly higher than for the other tests. The measured voltage degradation for tests B–F is comparable both with respect to the total voltage drop (Table 1) and the trend for the cell voltage curve over time (Fig. 1).

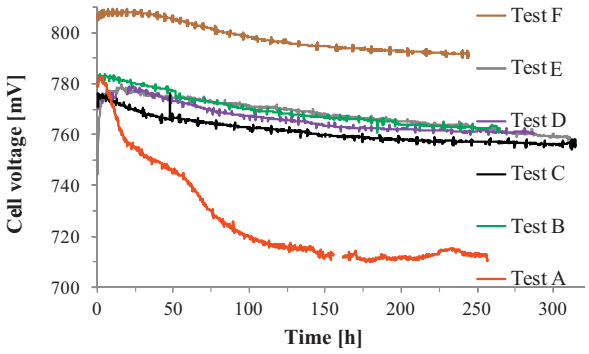

Fig. 1. Cell voltage curve over time (Table 1). The fuel cell testing was done at a temperature of 750 °C and a current density of 0.75 A cm^{-2}. The flow to the cathode was O_2 and the flow to the anode was 40% H_2O in H_2 (26% H_2 utilization). Cell voltage curve for tests C–E was added 13 mV, 15 mV and 11 mV, respectively, due to larger R_s values (see text for details).

3.1. *Effect of pre-treatment at 4% H_2O in H_2 at OCV – test C*

To investigate *whether or not* the steam content for this OCV pre-treatment plays a role for the subsequent fuel cell test results, a test (test C) was performed where the OCV pre-treatment was done at 4% H_2O in H_2 and otherwise same conditions as for test B (OCV pre-treatment at 40% % H_2O in H_2). Furthermore, a steam content of 4% is a more typical applied fuel cell test condition than 40% H_2O in the inlet gas to the anode. Fig. 2 shows the first and last IS recorded during this OCV pre-treatment at 750 °C, 4% H_2O in H_2 to the anode and oxygen to the cathode. The lines represent the results from optimal CNLS fitting of the experimental data applying the equivalent circuit model described in Section 2. By simple visual inspection of the IS in Fig. 2 it is evident that R_s has increased slightly, but the main change has occurred for the polarization resistance at a frequency of 2–3 kHz, which indicate an increase in the charge transfer reaction resistance in the Ni/YSZ electrode [22]. Table 2 summarizes the results (i.e. resistances and summit frequencies) from the CNLS fitting shown in Fig. 2.

After OCV pre-treatment fuel cell testing was started. Fig. 3 shows the first and last IS recorded during this fuel cell testing for test C. The lines represent the results from optimal CNLS fitting of the experimental data applying the equivalent circuit model described in Section 2. Table 3 summarizes the results

Table 2
Resistances and summit frequencies obtained from CNLS fit of first (1 h) and last (435 h) IS during pre-treatment at 4% H_2O in H_2 at OCV and 750 °C prior to fuel cell test C. Equivalent circuit model described by Barfod et al. was applied [22,35]. Estimated errors for obtained resistances are ~0.002 Ω cm².

Test C (OCV)	R_s [Ω cm²]	$R_{LSM,high}$ [Ω cm²]	$f_{s,LSM,high}$ [Hz]	$R_{Ni,TPB}$ [Ω cm²]	$f_{s,Ni,TPB}$ [Hz]	$R_{LSM,low}$ [Ω cm²]	$f_{s,LSM,low}$ [Hz]	$R_{diff.}$ [Ω cm²]	$f_{s,diff}$ [Hz]	$R_{conv.}$ [Ω cm²]	$f_{s,conv.}$ [Hz]
1 h	0.136	0.079	32,816	0.179	2859	0.062	542	0.002	43	0.015	4
435 h	0.150	0.082	30,007	0.255	2003	0.064	403	0.002	31	0.016	4

Table 3
Resistances and summit frequencies obtained from CNLS fit of first and last IS during test A–F at 750 °C and a current density of 0.75 A cm⁻². The flow to the cathode was O_2 and the flow to the anode was 40% H_2O in H_2 (26% H_2 utilization). Equivalent circuit model described by Barfod et al. was applied [22,35]. Estimated errors for obtained resistances are ~0.002 Ω cm².

Test no.	R_s [Ω cm²]	$R_{LSM,high}$ [Ω cm²]	$f_{s,LSM,high}$ [Hz]	$R_{Ni,TPB}$ [Ω cm²]	$f_{s,Ni,TPB}$ [Hz]	$R_{LSM,low}$ [Ω cm²]	$f_{s,LSM,low}$ [Hz]	$R_{diff.}$ [Ω cm²]	$f_{s,diff}$ [Hz]	$R_{conv.}$ [Ω cm²]	$f_{s,conv.}$ [Hz]
Test A, 1 h	0.094	0.064	23,735	0.061	5015	0.031	662	0.003	24	0.011	5
Test A, 256 h	0.088	0.064	17,386	0.123	2145	0.030	401	0.002	70	0.006	5
Test B, 1 h	0.085	0.063	22,719	0.064	5116	0.030	761	0.003	46	0.010	4
Test B, 264 h	0.077	0.063	22,539	0.066	4220	0.048	470	0.003	63	0.015	3
Test C, 1 h	0.112	0.063	22,956	0.069	8077	0.030	1014	0.002	138	0.015	7
Test C, 312 h	0.101	0.063	23,858	0.069	6321	0.057	902	0.002	226	0.013	6
Test D, 17 h	0.114	0.064	23,665	0.058	7959	0.040	822	0.004	25	0.013	5
Test D, 275 h	0.101	0.064	24,252	0.063	6235	0.058	521	0.004	29	0.014	4
Test E, 1 h	0.108	0.064	24,444	0.064	7215	0.039	1008	0.003	173	0.014	4
Test E, 297 h	0.092	0.064	24,264	0.070	5967	0.057	543	0.003	213	0.014	4
Test F, 1 h	0.099	0.062	21,175	0.028	7922	0.026	1250	0.004	70	0.026	8
Test F, 243 h	0.093	0.062	21,192	0.043	5212	0.031	1223	0.004	78	0.019	9

(i.e. resistances and summit frequencies) from the CNLS fitting shown in Fig. 3. From simple visual inspection of the spectra in Fig. 3, it is evident that R_s decreased slightly during test C and R_p increased. The main increase in R_p occurs at a frequency of ~1 kHz and the development of the IS in Fig. 3 is very similar to the IS previously reported for test B [19]. Furthermore, it can be noticed that even though the Ni/YSZ passivate (increase in $R_{Ni/YSZ}$) during the OCV pre-treatment, the anode seems fully activated

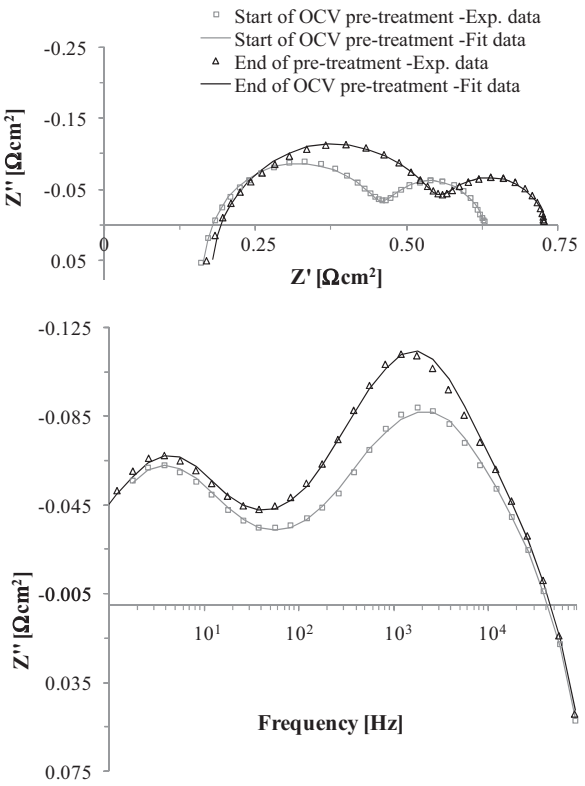

Fig. 2. First (□, 1 h) and last (Δ, 435 h) IS recorded during pre-treatment at 40% H_2O in H_2 at OCV and 750 °C prior to fuel cell test C. Lines are fitted spectra. Results from optimal CNLS fit are summarized in Table 2 and based on the equivalent circuit model described by Barfod et al. [22,35].

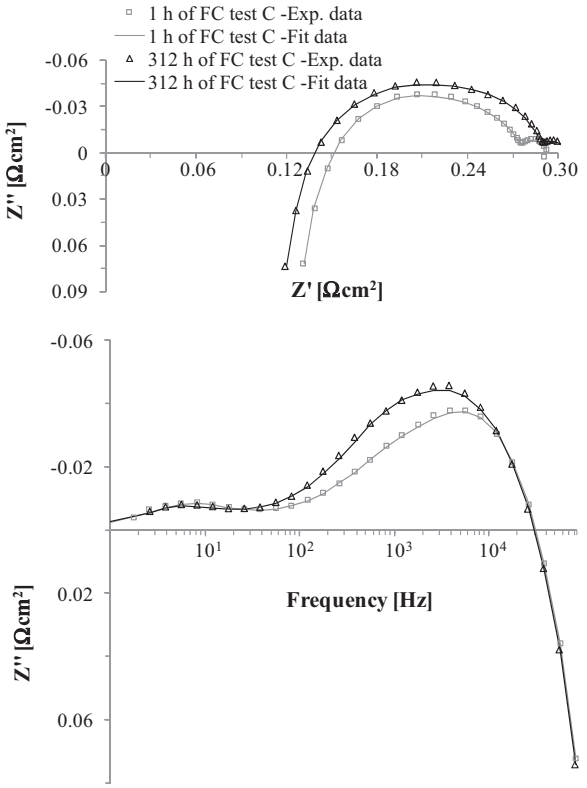

Fig. 3. First (□, 1 h) and last (Δ, 312 h) IS recorded during fuel cell test C at a temperature of 750 °C and a current density of 0.75 A cm⁻² after pre-treatment at OCV and 4% H_2O in H_2. The flow to the cathode was O_2 and the flow to the anode was 40% H_2O in H_2 (26% H_2 utilization). Lines are fitted spectra. Results from optimal CNLS fit are summarized in Table 3 and based on the equivalent circuit model described by Barfod et al. [22,35].

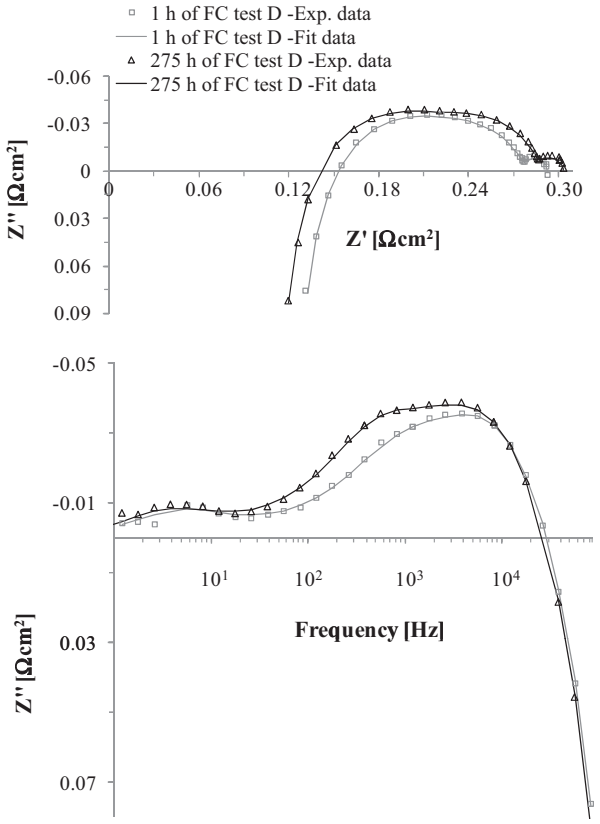

Fig. 4. First (□, 1 h) and last (Δ, 275 h) IS recorded during fuel cell test D at a temperature of 750 °C and a current density of 0.75 A cm^{-2} applying H_2 gas cleaning at 700 °C. The flow to the cathode was O_2 and the flow to the anode was 40% H_2O in H_2 (26% H_2 utilization). Lines are fitted spectra. Results from optimal CNLS fit are summarized in Table 3 and based on the equivalent circuit model described by Barfod et al. [22,35].

upon start of fuel cell test C (Table 3) as it was also observed for test B.

3.2. Effect of H_2 gas cleaning at 700 °C – test D

For test D the inlet H_2 was cleaned by leading the gas over porous Ni at 700 °C prior to leading the gas to the anode compartment of the cell. Fig. 4 shows the first and last IS recorded during test D. The lines represent the results from optimal CNLS fitting of the experimental data applying the equivalent circuit model described in Section 2. Table 3 summarizes the results (i.e. resistances and summit frequencies) from the CNLS fitting shown in Fig. 4. The trends for the development of the IS for test D are somewhat similar to those observed for test C, however the main increase in the polarization resistance seem to occur at a slightly lower frequency (~600 Hz) for test D compared to test C.

In general gas change impedance analyses were performed before and after each fuel cell test periods to make an electrode-specific and model-independent complementary check of the analysis results obtained by CNLS fitting for IS recorded during fuel cell testing. Fig. 5 provides an example of the results for such a gas change analysis for test D from which it can be observed that both the cathode and anode response to these differences upon gas changes (see Section 2 for details) has only changed slightly upon fuel cell test D. Another point to notice from the gas change impedance analysis depicted in Fig. 5 is that the responses to the gas change occur at a slightly lower frequency after fuel cell testing. This seems to be a general trend for the gas change analyses in this work and supports the findings regarding summit frequencies presented in Table 3. Fig. 6 shows the first and last IS recorded during test E (by-passing the gas cleaning system after test D). The lines represent the results from optimal CNLS fitting of the experimental data applying the equivalent circuit model described in Section 2. Table 3 summarizes the results (i.e. resistances and summit frequencies) from the CNLS fitting shown in Fig. 6. The trends for the development of the IS for test E (without gas cleaning) are very similar as those observed for test D (gas cleaning at 700 °C).

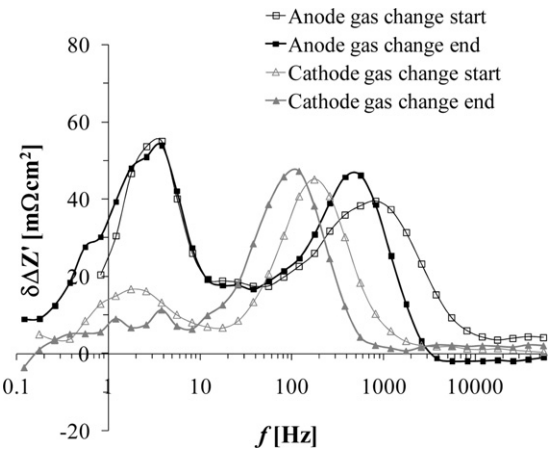

Fig. 5. Gas change impedance characterization at OCV, 750 °C prior to and after test D (gas cleaning at 700 °C). Four IS were recorded both before and after fuel cell testing, i.e. IS at p(H_2O) = 0.04 atm or p(H_2O) = 0.20 atm in H_2 applying air or O_2 to the cathode. From these IS $\delta\Delta Z'(f)$ was calculated as given by Eq. (1) [32].

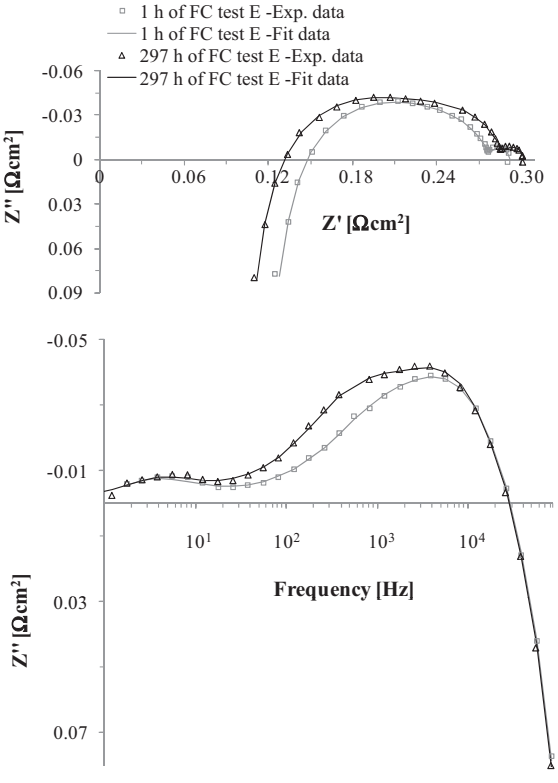

Fig. 6. First (□, 1 h) and last (Δ, 297 h) IS recorded during fuel cell test E at a temperature of 750 °C and a current density of 0.75 A cm^{-2} without H_2 gas cleaning after test D where H_2 gas cleaning at 700 °C was applied. The flow to the cathode was O_2 and the flow to the anode was 40% H_2O in H_2 (26% H_2 utilization). Lines are fitted spectra. Results from optimal CNLS fit are summarized in Table 3 and based on the equivalent circuit model described by Barfod et al. [22,35].

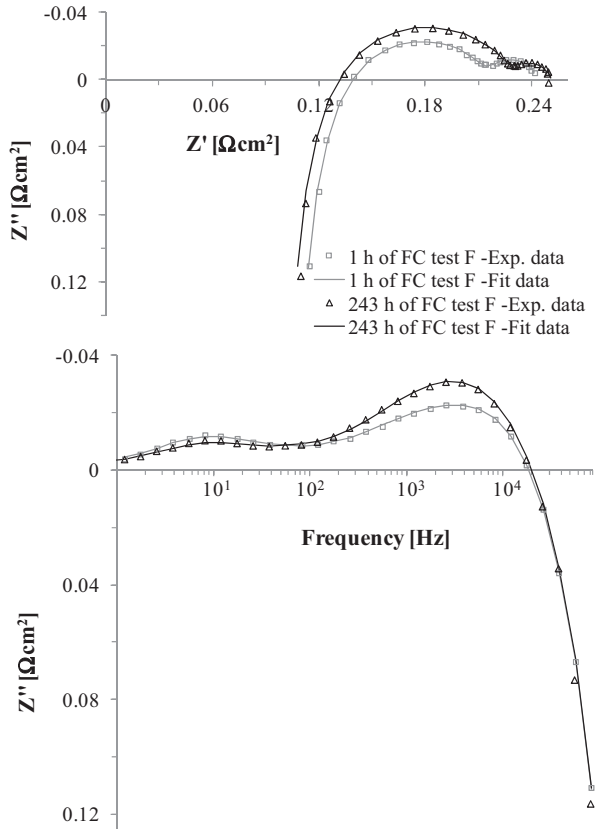

Fig. 7. First (□, 1 h) and last (Δ, 243 h) IS recorded during fuel cell test F at a temperature of 750 °C and a current density of 0.75 A cm^{-2}. The flow to the cathode was O_2 and the flow to the anode was 40% H_2O in H_2 (26% H_2 utilization). Lines are fitted spectra. Results from optimal CNLS fit are summarized in Table 3 and based on the equivalent circuit model described by Barfod et al. [22,35].

3.3. Effect of processing via multilayer tape casting of anode half cell – test F

An alternative way of pre-treating the Ni/YSZ electrode of the SOFC is by changing the processing procedure for the anode half cell production. This was done for the cell used for test F where a multilayer tape casting procedure for the entire anode half cell production was applied (see "Section 2"). The initial anode performance increase obtained by multilayer tape casting of the anode half cell is described elsewhere [36]. No OCV pre-treatment was applied or gas cleaning of the inlet H_2 was applied for test F; and the test specifications for test F are therefore identical to the test specifications for the reference test A. Fig. 7 shows the first and last IS recorded during test F (multilayer tape cast cell). The lines represent the results from optimal CNLS fitting of the experimental data applying the equivalent circuit model described in Section 2. Table 3 summarizes the results (i.e. resistances and summit frequencies) from the CNLS fitting shown in Fig. 7. As this cell from a production point of view is different from the other tested cells, it is worthwhile to check whether the arcs in the impedance response from the anode of this cell occur at frequencies similar to those for the other cells. Ideally this check of frequency for the anode response should be done without applying an equivalent model, i.e. model-independent. Therefore, gas change analysis for test F before and after fuel cell testing is shown in Fig. 8. Comparing the gas change analysis results from tests D and F, it is observed that the responses to the gas changes for the cell used for test F is at similar frequencies as observed for the cells used for tests A–E.

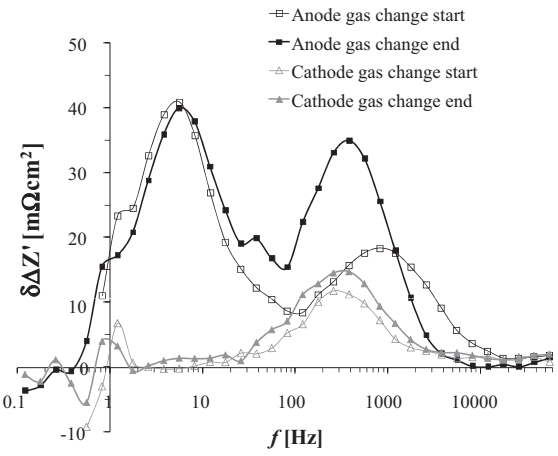

Fig. 8. Gas change impedance characterization at OCV, 750 °C prior to and after test F (multilayer tape cast cell). Four IS were recorded both before and after fuel cell testing, i.e. IS at $p(H_2O) = 0.04$ atm or $p(H_2O) = 0.20$ atm in H_2 applying air or O_2 to the cathode. From these IS $\delta\Delta Z'(f)$ was calculated as given by Eq. (1) [32].

3.4. SEM results

Fig. 9 shows representative low voltage in-lens SEM images of a non-tested but reduced cell (Fig. 9a), the cell from the reference test A (Fig. 9b), the cell from the OCV pre-treated test B (Fig. 9d) and the cell from test F (Fig. 9e). Using this low voltage in-lens SEM imaging technique, the percolating Ni particles will appear bright in the images [33]. From simple visual inspection of the SEM images in Fig. 9 it is evident that the quantity of percolating Ni is significantly lower both in the active anode and in the support layer for the cell from test A, when compared to a "fresh", reduced but non-long-term tested cell (Fig. 9a). Fig. 9c shows a magnification of the anode of the cell used for test A and from this SEM image it is evident that there are significant quantities of non-percolating Ni in this anode. Non-percolating Ni as illustrated in Fig. 9c was found both in the active anode and the support layer for the cell used for test A. Furthermore, it can be observed that the OCV pre-treated cell from fuel cell test B (Fig. 9d) has a Ni percolating network similar to the non-tested cell (Fig. 9a), indicating a "preservation" of the percolating Ni network after OCV treatment and fuel cell testing for test B. When only looking at the Ni percolating network, the active anode and anode support layer for the cell used for test F (multilayer tape cast half cell) in Fig. 9e looks similar to both the non-tested but reduced cell (Fig. 9a) and the cell from test B (Fig. 9d). However, the multilayer tape cast cell can differ from these cells when it comes to other microstructural parameters e.g. Ni particle size distribution and porosity. Table 4 gives the area fractions of percolating Ni in the active anode and support layer for the reduced, non-long-term tested reference cell and the cells from test A, B and F. The numbers given in Table 4 confirm the qualitative statements regarding the percolating Ni network given above for Fig. 9a,

Table 4
Area fraction of percolating Ni in the active anode and the support layer. The area fractions of percolating Ni is given as percentage of the total surface area and based on analysis of low voltage in-lens SEM images in Fig. 9 and similar supplementary images for each of the cells. Estimated precision for the obtained area fractions of percolating Ni is ±2%.

Test no.	Active anode [%]	Analyzed area [μm²]	Anode support layer [%]	Analyzed area[μm²]
Ref. cell	37	4845	33	12,997
Test A	27	1242	24	6735
Test B	41	5405	34	18,821
Test F	36	11,982	29	5211

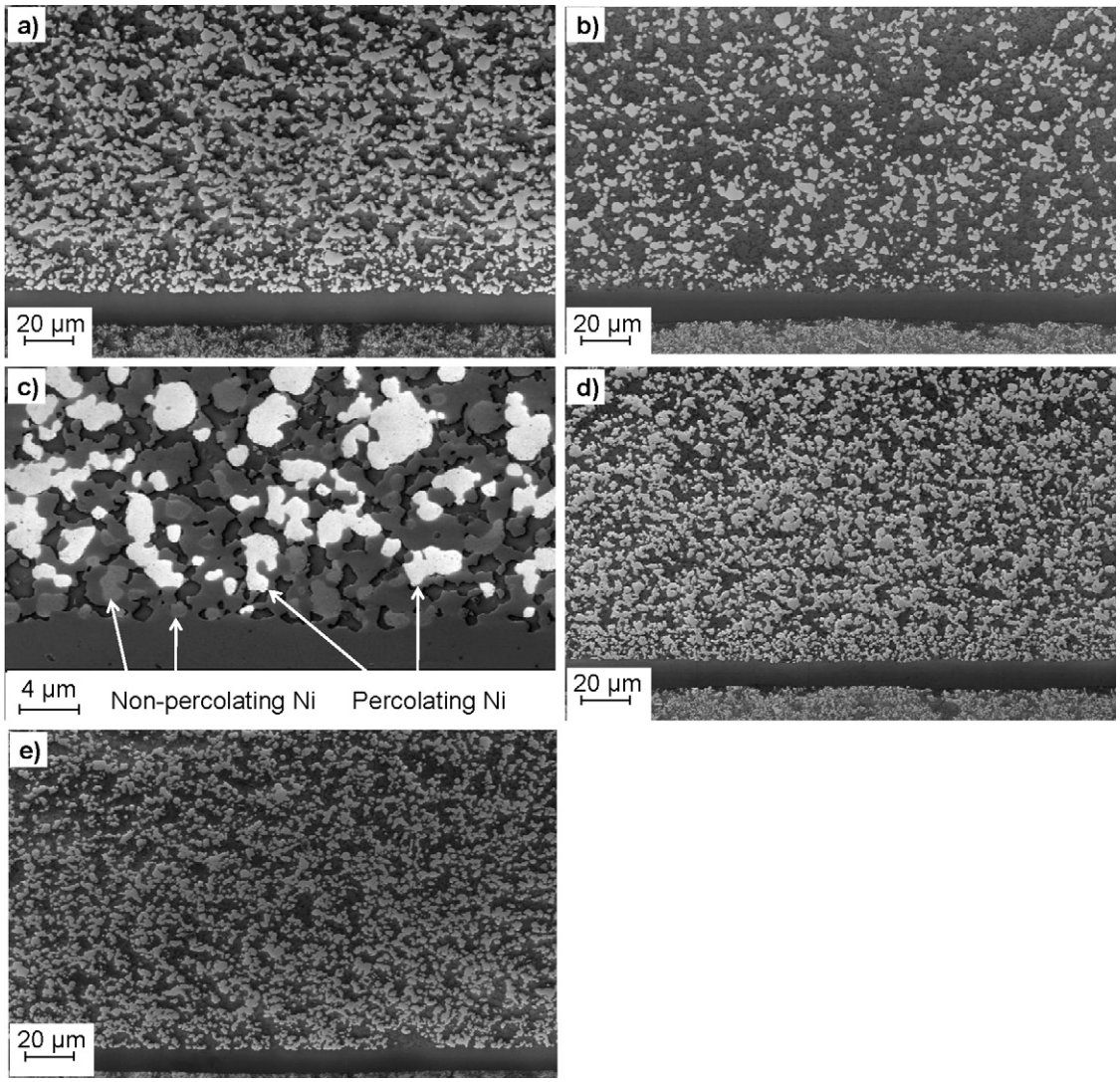

Fig. 9. Representative low-voltage in-lens SEM images. (a) Overview image of a reference cell where the NiO was reduced but the cell was not subjected to long-term fuel cell testing. (b) Overview image the cell from test A. (c) Higher magnification image of the cell from test A showing percolating and non-percolating Ni in the active anode layer. (d) Overview image of the cell from test B. (e) Overview image of the cell from test F.

b, d and e. For the numbers in Table 4 images from both gas inlet and outlet regions of the different cells were analyzed. The differences for the area fraction of percolating Ni when comparing a gas inlet part and a gas outlet part of a cell were within the estimated precision of approximately ±0.02%.

4. Discussion

The test results presented in the previous section should be compared with and discussed in relation to previously reported Ni/YSZ degradation studies for similar cells [13,19]. In these articles the effect of variation of $p(H_2O)$, the effect of current density, the effect of pre-treatment at OCV with 40% steam in H_2; and the effect of gas cleaning at room temperature on the Ni/YSZ degradation was reported, but post-mortem analysis via SEM imaging was not included for any of the tested cells.

4.1. Pre-treatment at OCV – wet and dry

Originally the OCV test period for test B was conducted to study the Ni/YSZ degradation at different current densities i.e. also at 0 A cm^{-2}. The previously reported [19] test B (OCV pre-treatment at 40% steam) clearly showed that the anode degraded even during this OCV test period but also revealed two surprising results: (1) the cell fully recovers from the passivation[1] that occurred during OCV testing upon start of fuel cell testing and (2) the Ni/YSZ electrode degradation during the 264 h of fuel cell testing was significantly lowered compared to a non-pre-treated cell (Table 3) [19]. It can be speculated what effect (if any) the relatively high partial pressure of steam during the OCV pre-treatment for test B can have, and this initiated test C reported here. The development of $R_{Ni,TPB}$ is different for test B (increased 130% over 440 h) compared to test C (increased 42% over 435 h) which is not surprising considering previously reported results, where it was shown that testing at OCV instead of under load prolonged the time frame for the $R_{Ni,TPB}$ increase, just as well as lowering the $p(H_2O)$ was shown to slow down the increase in $R_{Ni,TPB}$ [13,19]. However, the pre-treatment at OCV and only 4% H_2O in H_2 have a similar beneficial effect on the development of $R_{Ni,TPB}$ during the subsequent fuel cell test (Fig. 1). In this study of OCV pre-treatment only the $p(H_2O)$ was changed,

[1] The term "passivation" is used to describe reversible or partly reversible losses in performance for the SOFC.

but as these studies have showed an interesting effect of the "pre-history" of the cell for the Ni/YSZ degradation during otherwise identical fuel cell test conditions, it could be worthwhile to consider a study of the time frame for such OCV pre-treatment.

4.2. Applying high temperature gas cleaning

Cleaning the inlet H_2 over porous Ni significantly decrease the Ni/YSZ electrode degradation during fuel cell testing (test D, Table 3). Comparing the decrease in cell voltage for test D in this work where the H_2 gas cleaning was performed at 700 °C with the cell voltage degradation for a test where the gas cleaning was done at room temperature ("Test B" in previously reported work [19]), it is observed that the high temperature gas cleaning works slightly better than room temperature gas cleaning with respect to decreasing the Ni/YSZ degradation. Room temperature gas cleaning will favor simple adsorption of impurities on Ni surfaces in the gas cleaning system, whereas operating the gas cleaning system at 700 °C will favor chemical reactions but on the other hand increase desorption of adsorbed species. The gas cleaning was intentionally operated at temperature slightly below (50 °C) the cell test temperature. From the test applying room temperature gas cleaning and the test D reported here, it is proposed that the effect of the H_2 gas cleaning system is not only due to simple adsorption of impurities on the porous Ni in the gas cleaning system but electrochemical reactions most likely also play a role in the cleaning of the inlet H_2. In principle an optimal gas cleaning temperature could be determined; however this will most likely be influenced by the composition of the impurities in the applied gas stream.

The results from test E (by-passing the gas cleaning system after test D where H_2 gas cleaning at 700 °C was applied, Fig. 6 and Table 3) shows that minimizing the quantities of external impurities supplied to the cell for the first couple of hundred of test hours (test D) has a very beneficial effect on the subsequent fuel cell test without gas cleaning. In this context even fuel cell testing (test D) itself can be considered a "pre-treatment" of the Ni/YSZ electrode. The increase in $R_{Ni,TPB}$ for tests D and E is alike (0.005 Ω cm^2 and 0.006 Ω cm^2, respectively) and significantly smaller than that obtained for reference test A (0.062 Ω cm^2). This could indicate that the observed, however small, $R_{Ni,TPB}$ increase for tests D and E is not an effect of "external" impurities supplied to the cell during testing.

4.3. Effect of changed initial Ni/YSZ electrode structure – multilayer tape cast cell

In principle, processing the Ni/YSZ electrode in a different way can be thought of as a pre-treatment of the electrode, in the sense that the Ni/YSZ electrode microstructure, and even nano-structure, can be expected to be different from the structure for the cells for tests A–E upon starting fuel cell testing. As reported previously the multilayer tape cast cell had significantly higher initial Ni/YSZ electrode performance and from the IS data analyses results given in Table 3 it is evident that also from a Ni/YSZ electrode degradation point of view, the multilayer tape cast cell used for test F is interesting. For comparison $R_{Ni,TPB}$ increased 62 mΩ cm^2 for reference test A, but only 15 mΩ cm^2 for test F over approximately 250 h even though they were tested at the same conditions with no pre-treatment and no gas-cleaning. It is worthwhile to emphasize that the raw materials, same ratios and layer thickness' were applied for the multilayer tape cast cell for test F as for the standard produced (tape cast anode support and sprayed active anode and electrolyte) cells used for tests A–E, i.e. decrease in the Ni/YSZ electrode degradation observed when comparing tests A and F can be assumed to be an effect of processing via multilayer tape casting and co-firing. Test F is the first durability testing for this initial work on multilayer tape casting of anode half cells in our laboratory, and therefore there is a lack of comprehensive test data including test of cells with varying processing parameters and electron microscopy characterization of tested and non-tested reference cells is not yet available. However, from the results from test F we suggest two issues to explain the promising results from the multilayer tape cast cell: (1) The multilayer tape casting process is made "wet-on-wet" for all three layers of the anode half cell or in other words the two interfaces anode support/active anode and active anode/electrolyte are produced "wet-on-wet" which from a qualitative point of view can be expected to improve the adhesion between the different layers in the anode half cell. (2) The Ni particle size distribution (PSD) is more optimal e.g. there are a greater fraction of smaller Ni particles. This potentially provides more triple-phase-boundaries per unit volume Ni/YSZ electrode. This can be part of the explanation for the higher initial performance, but if this is the case, then the lower increase in $R_{Ni,TPB}$ for test F compared to test A (and several other tests of similar cells [12,13]) indicates that this optimized Ni PSD is also more stable. Additional SEM work and image analysis on the cell from test F, and non-tested reference multilayer tape cast cell, etc. is necessary to support or disregard the proposed explanations.

4.4. Microstructural changes

Before discussing the SEM results presented in Fig. 9, it is worthwhile shortly to discuss the sample preparation and the imaging technique including the process for image analyses. It can be argued that when breaking off a piece of cell for SEM, this breakage of the cell will occur along a mechanically not so strong interface in the cell, and therefore this fracture might not be a representative structure. However the cell piece is subsequently grinded and polished and the cross section for SEM imaging can therefore be assumed to be random and representative for the cell microstructure. There are two main issues associated with the measurement of the percolating Ni fraction by the previously described image analysis method. No ground truth is available for the segmentation of the images and the percolation images do not take into account percolation through pathways in the part of the sample that has been polished away. These two effects combined means that the *accuracy* of the measurements is unknown. The measurement *precision* is however high (approximate ±0.02, Table 4) due to the same reproducible methodology being applied to all samples. The measured percolating Ni fraction should thus be valid for a comparative study between the different tests in this work since the unknown accuracy error is expected to be similar for all samples. However, one should be careful when comparing the numbers given in Table 4 with similar numbers given in literature.

In the "*Results*" section only SEM images of the cells used for test A, B, F and a non-fuel-cell tested reference cell was included. This selection of cells for microscopy was based on the fact that from a cell production point of view the cells from tests A–E are alike whereas the multilayer tape cast cell is different, and the observed degradation for tests C–E seem somewhat similar to that observed for test B. The difference in the fraction of percolating Ni both in the active anode and in the anode support between the cell used for tests A and B (Fig. 9) is striking, and the SEM results fit well with the cell voltage degradation (Fig. 1) and especially the results from CNLS fitting of the IS recorded during fuel cell testing (Table 3). Furthermore, it should be noted that the cells from tests A and B are "sister cells". This means that 5 cm × 5 cm cells have been cut out of two neighboring 12 cm × 12 cm cells of the tape which should ensure the highest degree of equality between the cells. It could be argued that the observed significant loss in Ni percolation for the cell used for test A could be a feature somehow specific for exactly this batch of cells. However, this is not the case. The cell described as "Test C" in our previous work [13] was operated with an inlet of 60% H_2O in H_2 but otherwise same conditions as for test A in

this work. This cell had a degradation behavior similar to test A, but the cell was from another production batch and year. The low voltage in-lens SEM imaging of this cell showed a similar decrease in the fraction of percolating Ni both in the active anode layer and in the support layer as observed for the cell used for test A in this work. From a first glance at the overview image of the cell used for test A (Fig. 9b) it seems like the content of Ni in the active anode and support layer has decreased significantly when compared to the non-fuel-cell tested reference cell (Fig. 9a). In principle loss of Ni could be due to evaporation of Ni species as described e.g. by Guebner [37]. However, a thermochemical calculations using FactSage® reveal that the activity of $p(Ni(OH)_2)$, which is by far most abundant volatile Ni-specie, is only 4×10^{-12} mole l^{-1}. The cells were operated with a total flow to the anode of approximately 31 l h^{-1} for approximately 250 h of test plus $\sim 2 \times 75$ h for characterization. From these numbers an estimate of the evaporated Ni will be $\sim 3 \times 10^{-6}$ g. One cell with the geometry and layer thicknesses as described in "Section 2" and Table 4 will contain ~1.3 g of Ni, which indicate that the estimated amount of evaporated Ni-species for test A can be considered negligible.

As illustrated by the larger magnification image of the electrolyte–anode interface for the cell used for test A (Fig. 9c), it is possible to locate significant quantities of non-percolating Ni in the anode from test A. The loss in Ni percolation can be due to nano-scaled layers of impurities between Ni particles, which will disconnect the electron conduction in the Ni network. Using energy dispersive spectroscopy (EDS) and field-emission SEM it was not possible to locate such impurities at the surfaces of the Ni particles in quantities significantly above the detection limit; however EDS at the SEM is not a proper analysis tool for such nano-scale – or even monolayer – features between Ni particles.

There are examples in literature providing 3D reconstructions of Ni/YSZ electrodes including determination of degree of percolating versus non-percolating TPB [17,38,39]. These results originate from 3D reconstructions of rather small cubes of Ni/YSZ electrode and from studies on pressed pellets and/or non-long-term tested cells and a direct quantitative comparison with the 2D SEM images and image analysis given in "Section 3" here are not proper. Another interesting work was presented by Tanasini et al. [16]. They modeled relations between anode degradation during fuel cell testing and the volumetric Ni fraction and discussed the Ni percolation threshold. Even though their modeling was based on operating the fuel cell at different conditions (850 °C, 0.5 A cm^{-2}, 3% H_2O in H_2) than those applied here, their results are relevant. They showed that at these conditions the development of anode overpotential changes significantly (more than 100 mV) even upon changing the fraction of Ni from 37% to 33%. In this context the numbers in Table 4 indicate that the fraction of percolating Ni in the cell used for test A might be below what can be considered a Ni percolation threshold. It looks significantly different for the cell used for test B (OCV pre-treatment, Fig. 9d) for which the fraction of the percolating Ni both in the active anode and support layer is at least as high as for the non-tested reference cell (Table 4). The high fraction of percolating Ni for the cell used for test B and observed minimal degradation (Fig. 1 and Table 3) fits well with the modeling work by Tanasini et al. [16].

4.5. Hypotheses for mechanisms

Based on the results presented and discussed above, it is clear that impurities in the gas stream play a role in the Ni/YSZ electrode degradation but also that operating the SOFC at OCV prior to fuel cell testing has a significant, and positive, effect on the Ni/YSZ electrode degradation in the subsequent fuel cell test even for non-cleaned H_2 inlet gas. In this paragraph we discuss three different test scenarios related to the test results presented, that is; *scenario 1*: A reference fuel cell test (e.g. test A); *scenario 2:* A test applying pre-treatment at OCV, but no gas cleaning (e.g. tests B and C); and *scenario 3:* A test applying gas cleaning at start of fuel cell testing and subsequent fuel cell testing without gas cleaning (e.g. tests D and E). In all three scenarios it is worthwhile to notice that upon start of testing at constant conditions, the surfaces and interfaces in the anode are hardly clean. Most likely impurities will be present on surfaces and at interfaces both at/on Ni and YSZ, and probably impurities having different compositions and properties at the different surfaces and interfaces [40–43].

In *scenario 1* (test A) we most likely start out with non-clean surfaces and interfaces, likely with glassy phase impurities. To this anode we lead non-cleaned gasses and upon starting the galvanostatic fuel cell testing a potential gradient as well as a gradient in the $p(H_2O)$ are applied. The external impurities build-up and block active TPB leading to the observed increase in $R_{Ni,TPB}$. Based on the SEM work for test A, it can be argued that impurities might also be present at two-phase boundaries.

In *scenario 2* (tests B and C) we have similar non-clean surfaces and interfaces upon start of OCV pre-treatment. During this OCV pre-treatment we lead similar impurities via the inlet gasses to the anode as for *scenario 1*,[2] but do not create potential and $p(H_2O)$ gradients. This possibly influences the build-up and mobility of external impurities at the TPB. During this OCV pre-treatment period it is likely that the internal impurities (e.g. in raw materials) will segregate to and/or re-arrange at surfaces and grain boundaries and there are possibilities for surface morphology changes [40,41,44–46]. Furthermore, based on previous electrolysis test results [21,27,47], we believe that it is possible that such re-organization of impurities during this OCV pre-treatment period can include build-up of crystals which are not covering the TPB as tight as the initial glass phase. Upon polarization of the cell i.e. start of fuel cell testing for *scenario 2,* the TPB will be freed ("outgoing" $p(H_2O)$ gradient) of impurities or at least no more TPB are covered by impurities than was the case for *scenario 1* upon start of fuel cell testing (notice: tests A and B have the same $R_{Ni,TPB}$ upon start of fuel cell testing). During the subsequent fuel cell testing in *scenario 2*, the re-organization of internal impurities and/or morphology changes that occurred during the OCV pre-treatment have provided a NiYYSZ electrode that seems more "immune" towards the external impurities from the gas stream. This could be related to crystals of impurities built-up during the OCV pre-treatment on which the impurities from the gas stream may grow more easily than at the TPB. Some of the glassy phase impurities that build-up during OCV may change composition and crystallize due to the $p(H_2O)$ gradient that arises at start of test.

In *scenario 3* (tests D and E) we apply potential and $p(H_2O)$ gradients from the start of testing at constant conditions, but we do not lead external impurities (or at least decrease the amount of impurities) to the anode as this first test period is operated applying cleaned H_2. This test period for *scenario 3,* we envisage, work as a "pre-treatment" period. Similar, but not identical, mechanisms as described above for the OCV pre-treatment period for *scenario 2* can occur in this part of *scenario 3*, e.g. internal impurities that segregate, re-organize and form crystals. This means that for the last part of *scenario 3* (by-passing the gas cleaning system), the anode is believed to have become more "immune" towards the impurities in principle somewhat like for *scenario 2*.

[2] It has previously been reported that the observed increase in $R_{Ni,TPB}$ during OCV pre-treatment at 40% H_2O in H_2 is also related to impurities in the gas stream. This is evident from the comparison of the development of $R_{Ni,TPB}$ over time for test D (no gas cleaning) and E (with gas cleaning) during OCV pre-treatment in our previously reported work [19].

Considering the proposed mechanisms above for tests A–E and the long-term test result for test F (multilayer tape cast cell), it is probable that the "wet-on-wet" multilayer tape casting of the anode half cell have led to surfaces, impurities and Ni morphology different from those of the cells used for tests A–E. This possibly makes the multilayer tape cast cell less prone to/more "immune" towards the build-up of external impurities at the active TPB. Even though tests B–F show very similar long term stability e.g. based on the cell voltage curves depicted in Fig. 1, it is, as indicated by *scenarios 2 and 3* described above, not necessarily the same mechanisms that proceed during these tests and lead to the observed results.

Hypotheses as described above may be difficult to verify. However, for *scenario 2* combining OCV pre-treatment with electrolysis testing might provide new pieces to the puzzle in understanding the positive effect that such OCV pre-treatment has on the Ni/YSZ electrode degradation during the subsequent test under current load. Further deep SEM/TEM and surface analyses may also help in revealing more detailed information regarding which processes that are taking place.

5. Conclusion

This work included testing of five anode supported SOFCs. All fuel cell testing was performed at 750 °C, 0.75 A cm^{-2}, O_2 to the cathode and $p(H_2O)/p(H_2) = 0.4/0.6$ to the anode. Comparing the Ni/YSZ electrode degradation observed from cell test results and subsequent equivalent modeling of IS from a "reference" test (test A) with tests where different pre-treatments, use of gas cleaning and changed anode half cell processing was applied, we can conclude that:

- For the reference test A, the Ni/YSZ charge transfer reaction resistance, $R_{Ni,TPB}$, increased from 0.061 Ω cm^2 to 0.123 Ω cm^2 over 256 h of fuel cell testing; i.e. an increase in $R_{Ni,TPB}$, of 0.062 Ω cm^2.
- Pre-treatment at OCV for 440 h decreased the change in $R_{Ni,TPB}$ significantly for the subsequent fuel cell test both when applying 40% H_2O in H_2 (test B) and 4% H_2O in H_2 (test C) during the OCV pre-treatment.
- Applying H_2 gas cleaning at 700 °C also led to a significant decrease in the degradation of the Ni/YSZ electrode (test D) over 258 h of testing and continuing testing on the same cell as test D, but without gas cleaning (test E) also only showed a minor increase in $R_{Ni,TPB}$ over the 297 h of testing.
- Comparing the increase in $R_{Ni,TPB}$ for test A–E (similar type of cells), it was reduced to ¼ or less for tests B–E when compared to reference test A.
- The cell with the multilayer tape cast anode half cell was tested (test F) without pre-treatment or gas cleaning. The cell had a higher initial anode performance and decreased Ni/YSZ degradation compared to reference test A. $R_{Ni,TPB}$ for test F increased from only 0.028 Ω cm^2 to 0.043 Ω cm^2 over 243 h of fuel cell testing i.e. an increase in $R_{Ni,TPB}$ of 0.015 Ω cm^2.

Pieces from a reduced but non-fuel-cell tested cell, the "reference" fuel cell test (test A), the 40% H_2O in H_2 OCV pre-treated cell (test B) and the multilayer tape cast cell (test F) was investigated by low voltage in-lens SEM imaging and we can conclude that:

- The area fraction of percolating Ni was 37 ± 2% and 33 ± 2% for the active anode and support layer, respectively, for the reduced but non-fuel-cell tested cell.
- For the reference fuel test A, having the largest decrease in Ni/YSZ electrode performance during testing, the fraction of percolating Ni was reduced to 27 ± 2% and 24 ± 2% for the active anode and support layer, respectively. A significant quantity of non-percolating Ni was found in test A.
- The area fraction of percolating Ni for the test applying OCV pre-treatment prior to fuel cell testing (test B) was 41 ± 2% and 34 ± 2% for active anode and support layer, respectively.
- The area fraction of percolating Ni for the test where the anode half cell was produced via multilayer tape casting (test F) was 36 ± 2% and 29 ± 2% for active anode and support layer, respectively.

Acknowledgements

The authors thank colleagues at Fuel Cell and Solid State Chemistry Division at Risø DTU for assistance and discussions, especially technician Henrik Henriksen and post doc Christopher Graves. The financial support from Danish Energy Technology Development and Demonstration Program via the project "*Fuel Cells Put to Work*", from The Program Commission on Sustainable Energy and Environment, The Danish Council for Strategic Research, via the SERC project (www.serc.dk), Contract No. 2104-06-0011 and from Energinet.dk under the project ForskEL 2010-1-10441 "Durable and Robust SOFC" is gratefully acknowledged.

References

[1] S.C. Singhal, Solid State Ionics 152 (2002) 405.
[2] F. Tietz, H.P. Buchkremer, D. Stover, Journal of Electroceramics 17 (2006) 701.
[3] D. Stover, U. Diekmann, U. Flesch, H. Kabs, W.J. Quadakkers, F. Tietz, I.C. Vinke, Proceedings – Electrochemical Society 99 (19) (1999) 812.
[4] S.D. Ebbesen, M. Mogensen, Electrochemical and Solid State Letters 13 (2010) D106.
[5] S.C. Singhal, K. Kendall, High Temperature Solid Oxide Fuel Cells. Fundamentals, Design, and Applications, Elsevier Ltd., Oxford, UK, 2004.
[6] A. Atkinson, S. Barnett, R.J. Gorte, J.T.S. Irvine, A.J. Mcevoy, M. Mogensen, S.C. Singhal, J. Vohs, Nature Materials 3 (2004) 17.
[7] K. Haga, S. Adachi, Y. Shiratori, K. Itoh, K. Sasaki, Solid State Ionics 179 (2008) 1427.
[8] Y. Matsuzaki, I. Yasuda, Solid State Ionics 132 (2000) 261.
[9] E.V. Tsipis, V.V. Kharton, Journal of Solid State Electrochemistry 12 (2008) 1367.
[10] C. Sun, U. Stimming, Journal of Power Sources 171 (2007) 247.
[11] Q.X. Fu, F. Tietz, Fuel Cells 8 (2008) 283.
[12] A. Hagen, R. Barfod, P.V. Hendriksen, Y.L. Liu, S. Ramousse, Journal of the Electrochemical Society 153 (2006) A1165.
[13] A. Hauch, M. Mogensen, A. Hagen, Solid State Ionics, doi:10.1016/j.ssi.2010.01.004.
[14] A. Hauch, S.H. Jensen, M. Mogensen, Solid State Electrochemistry, in: Proceedings of the 26th Risoe International Symposium on Materials Science, 2005, p. 203.
[15] A. Faes, A. Hessler-Wyser, D. Presvytes, C.G. Vayenas, J. Van Herle, Fuel Cells 9 (2009) 841.
[16] P. Tanasini, M. Cannarozzo, P. Costamagna, A. Faes, J. Van Herle, A. Hessler-Wyser, C. Comninellis, Fuel Cells 9 (2009) 740.
[17] L. Holzer, B. Munch, B. Iwanschitz, M. Cantoni, T. Hocker, T. Graule, Journal of Power Sources, doi:10.1016/j.jpowsour.2010.08.006.
[18] S.D. Ebbesen, C. Graves, A. Hauch, S.H. Jensen, M. Mogensen, Journal of the Electrochemical Society 157 (2010) B1419.
[19] A. Hauch, M. Mogensen, Solid State Ionics 181 (2010) 745.
[20] P.H. Larsen, C. Bagger, S. Linderoth, M. Mogensen, S. Primdahl, M.J. Jorgensen, P.V. Hendriksen, B. Kindl, N. Bonanos, F.W. Poulsen, K.A. Maegaard, Proceedings – Electrochemical Society 2001 (16) (2001) 28.
[21] A. Hauch, S.D. Ebbesen, S.H. Jensen, M. Mogensen, Journal of the Electrochemical Society 155 (2008) B1184.
[22] R. Barfod, M. Mogensen, T. Klemenso, A. Hagen, Y.L. Liu, P.V. Hendriksen, Journal of the Electrochemical Society 154 (2007) B371.
[23] S. Ramousse, M. Menon, K. Brodersen, J. Knudsen, U. Rahbek, P.H. Larsen, ECS Transactions 11 (2007) 317.
[24] C. Bagger, Fuel Cell Seminar (1992) 241.
[25] M.J. Jorgensen, M. Mogensen, Journal of the Electrochemical Society 148 (2001) A433.
[26] P.H. Larsen, K. Brodersen, Patent US2008124602-A1, 2008.
[27] A. Hauch, S.H. Jensen, M. Mogensen, S. Ramousse, Journal of the Electrochemical Society 153 (2006) A1741.
[28] M. Mogensen, P.V. Hendriksen, in: S.C. Singhal, K. Kendall (Eds.), High Temperature Solid Oxide Fuel Cells – Fundamentals, Design and Applications, Elsevier Ltd., Oxford, UK, 2004.
[29] S.D. Ebbesen, M. Mogensen, Journal of Power Sources 193 (2009) 349.

[30] A. Hauch, Solid Oxide Electrolysis Cells – Performance and Durability, PhD Thesis, Risø National Laboratory, Technical University of Denmark, Roskilde, Denmark, 2007.
[31] D. Johnson, Zview 2.8, Scribner Associates Inc., 2003.
[32] S.H. Jensen, A. Hauch, P.V. Hendriksen, M. Mogensen, N. Bonanos, T. Jacobsen, Journal of the Electrochemical Society 154 (2007) B1325.
[33] K. Thydén, Y.-L. Liu, J.B. Bilde-Sorensen, Solid State Ionics 178 (2008) 1984.
[34] J.R. Rostrup-Nielsen, Steam reforming Catalysts. An Investigation of Catalysts for Tubular Steam Reforming of Hydrocarbons, Copenhagen, Denmark, 1975.
[35] R. Barfod, A. Hagen, S. Ramousse, P.V. Hendriksen, M. Mogensen, in: 6th European Solid Oxide Fuel Cell Forum Proceedings, 2004, p. 960.
[36] A. Hauch, K. Brodersen, M. Wandel, Journal of Power Sources, submitted for publication.
[37] A. Guebner, The Electrochemical Society Proceedings Series 97 (07) (1997) 844.
[38] P.R. Shearing, J. Golbert, R.J. Chater, N.P. Brandon, Chemical Engineering Science 64 (2009) 3928.
[39] J.R. Wilson, W. Kobsiriphat, R. Mendoza, H.-Y. Chen, J.M. Miller, D.J. Miller, K. Thornton, P.W. Voorhees, S.B. Adler, S.A. Barnett, Nature Materials 5 (2006) 541.
[40] A.E. Hughes, S.P.S. Badwal, Solid State Ionics 46 (1991) 265.
[41] M. de Ridder, A.G.J. Vervoort, R.G. van Welzenis, H.H. Brongersma, Solid State Ionics 156 (2003) 255.
[42] S.P.S. Badwal, Solid State Ionics 76 (1995) 67.
[43] M. Mogensen, K.V. Hansen, in: W. Vielstich, H. Yokokawa, H.A. Gasteiger (Eds.), Handbook of Fuel Cells – Fundamentals, Technology and Applications, John Wiley & Sons Ltd., 2009.
[44] K.V. Hansen, K. Norrman, M. Mogensen, Journal of the Electrochemical Society 151 (2004) A1436.
[45] M.S. Schmidt, K.V. Hansen, K. Norrman, M. Mogensen, Solid State Ionics 179 (2008) 1436.
[46] D. Lybye, Y.L. Liu, Journal of the European Ceramic Society 26 (2006) 599.
[47] A. Hauch, J. Bowen, L. Theil-Kuhn, M. Mogensen, Electrochemical and Solid-State Letters 11 (2007) B38.